J. Astrophys. Astr. (2014) **35,** 143–156

Multicolour CCD Photometric Study of Galactic Star Clusters SAI 63 and SAI 75

R. K. S. Yadav[1,*], S. I. Leonova[2], R. Sagar[1] & E. V. Glushkova[2]
[1]*Aryabhatta Research Institute of Observational Sciences (ARIES), Manora Peak, Nainital 263 129, India.*
[2]*Sternberg Astronomical Institute, Moscow Lomonosov State University, Universitetsky pr. 13, Moscow 119992, Russia.*
[*]*e-mail: rkant@aries.res.in*

Received 6 February 2014; accepted 30 April 2014

Abstract. We present *UBVI* CCD photometric observations obtained in the field of open clusters SAI 63 and SAI 75. CCD optical data obtained for the first time for these clusters are used to derive the fundamental parameters of the clusters. Stellar surface density profile indicates that radii of SAI 63 and SAI 75 are $\sim 3'.5$ and $2'.5$ respectively. The reddenings $E(B-V)$ are 0.44 ± 0.05 and 0.34 ± 0.05 mag for SAI 63 and SAI 75 respectively while the corresponding distances are 2.2 ± 0.2 and 3.5 ± 0.3 kpc. An age of 450 ± 50 Myr for SAI 63 and 90 ± 10 Myr for SAI 75 is determined using the theoretical isochrones of $Z = 0.019$. Our analysis shows that reddening law is normal towards SAI 75.

Key words. Hertzsprung–Russell (H–R) diagram—dust extinction—open clusters and associations: individual: SAI 63—open clusters and associations: individual: SAI 75.

1. Introduction

Studies of open star clusters help us to understand the galactic structure, star formation processes and stellar evolution. Among the various objects routinely used to study the galactic structure, galactic open clusters offer the advantage that it is relatively easy to estimate their ages and distances (Carraro *et al.* 2013). By using the colour–magnitude (CMD) and colour–colour diagrams of star clusters, it is possible to determine the underlying properties of clusters such as age, distance, reddening and metal abundance (Table 1). These parameters, in turn, can help to constrain the theories of star formation, and dynamical and stellar evolution in star clusters.

The JHK_s photometric data obtained from 2MASS survey have proved to be a fertile ground in the search for new open clusters. Recently, more than thousands of open clusters were discovered by analysing 2MASS data (Kronberger *et al.* 2006; Froebrich *et al.* 2007; Koposov *et al.* 2008; Glushkova *et al.* 2010). The reality of these newly discovered open clusters was confirmed by means of their J, $(J-H)$ and K_s, $(J-K_s)$ CMDs. Unfortunately, the 2MASS sensitivity is 15.8 mag for

Table 1. Basic parameters of the clusters under investigation. The equatorial co-ordinates of J2000.0, diameter, reddening, distance and age of the clusters are taken from http://ocl.sai.msu.ru/catalog/.

Name	α_{2000} (hh:mm:ss)	δ_{2000} (dd:mm:ss)	l (deg)	b (deg)	Dia. ($'$)	$E(B-V)$ (mag)	Distance (pc)	log(age)
SAI 63	06:13:44.5	+06:56:58	202.4	−5.1	4	0.37 ± 0.13	1910 ± 80	8.65 ± 0.05
SAI 75	07:15:22.5	−07:25:20	222.3	1.9	4	0.23 ± 0.03	2800 ± 330	< 8.6

J-band, 15.1 mag for H-band and 14.3 mag for K_s at $S/N = 10$, so for the majority of clusters, only the upper part of their CMD can be analysed. Therefore, cluster parameters derived using J, H and K_s data need to be verified by utilizing CCD observations in optical passbands.

Considering the above we decided to study two open clusters SAI 63 and SAI 75 selected from the Sternberg Astronomical Institute Open Cluster Catalog (SAI OCL catalogue). The above star clusters were discovered using 2MASS JHK_s data (Glushkova *et al.* 2010). CCD data for these clusters are obtained for the first time. The aim of the present analysis is to estimate the fundamental parameters of the clusters using *UBVI* CCD photometric data. Photometric diagrams using the present data set, provide an opportunity to perform detailed analysis of these objects, and estimate the fundamental parameters like size, reddening, distance and age of the clusters under study.

The article is organized as follows: In section 1, we provide the introduction while section 2 describes the acquired data set, their reduction procedure and calibration. Section 3 introduces the basic diagrams we use to extract cluster's fundamental parameters. Finally, section 4 summarizes the findings of this article.

2. Observations and reductions

We used CCD imaging to obtain *UBVI* photometry of the stars in the region of the open clusters SAI 63 and SAI 75. The data were obtained using the 2 K×2 K CCD system at the $f/13$ Cassegrain focus of the 104-cm Sampurnanand telescope of ARIES, Nainital, India. The 0.36 arcsec pixel^{-1} plate scale resulted in a total field-of-view of 12.3×12.3 arcmin^2. The readout noise and gain of the CCD are 5.3 e$^-$ and 10 e$^-$ ADU^{-1} respectively. Deep exposures were taken in each passband for accurate photometric measurements of fainter stars. Furthermore, observations were taken in 2×2 pixel binning mode to improve the signal-to-noise ratio (S/N) for relatively fainter stars. Observational information alongwith the date of observations are listed in Table 2. The identification maps of the clusters under study are shown in Fig. 1.

Bias and flat-field frames were taken during observations. Flat-field exposures were taken of the twilight sky in each filter. Bias and flat-field corrections were performed using the standard IRAF.[1] The DAOPHOT/ALLSTAR (Stetson 1987, 1992)

[1]IRAF is distributed by the National Optical Astronomical Observatory which are operated by the Association of Universities for Research in Astronomy, under contract with the National Science Foundation.

Table 2. Log of observations, with filters and exposure times information. SAI 63 was observed on February 03, 2011 while SAI 75 was observed on January 22, 2010.

Objects	Filters	Exposure time (in seconds)
SAI 63	*U*	1500 × 1, 300 × 1
	B	1200 × 2, 180 × 2
	V	900 × 2, 120 × 2
	I	300 × 2, 60 × 2
SAI 75	*U*	1200 × 2, 300 × 1
	B	900 × 2, 240 × 1
	V	600 × 2, 180 × 1
	I	300 × 2

package was used to derive instrumental magnitudes. Quadratically varying Point Spread Functions (PSFs) were used to derive instrumental magnitudes. The magnitudes have been aligned to that of a deepest frame for each filter and the final catalogue have been created including all the objects identified in at least two filters. To transform instrumental magnitude into the standard system, we observed standard field Rubin 149 for SAI 63 and PG0918 + 029 (Landolt 1992) for SAI 75.

The calibration equations used in transformation from instrumental to standard system were

$$\begin{aligned} u &= U + A_0 + A_1 \times (U - B) + A_2 \times X, \\ b &= B + B_0 + B_1 \times (B - V) + B_2 \times X, \\ v &= V + C_0 + C_1 \times (B - V) + C_2 \times X, \\ i &= I + D_0 + D_1 \times (V - I) + D_2 \times X, \end{aligned}$$

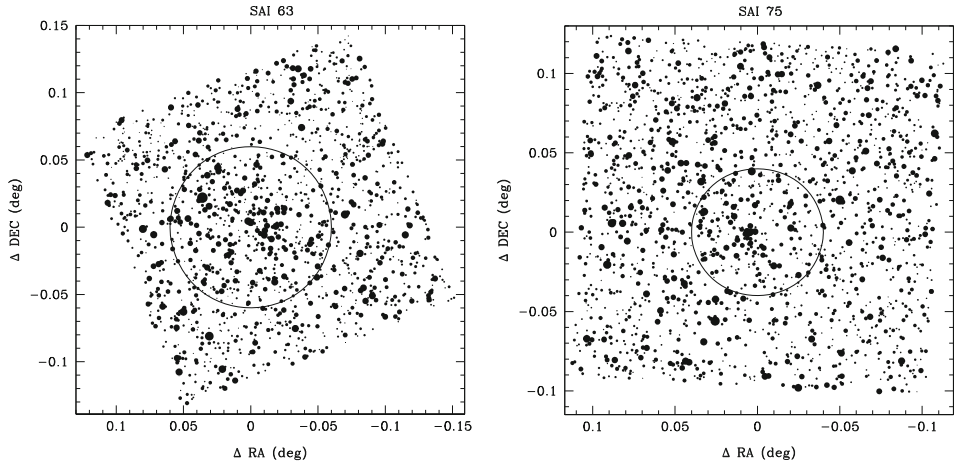

Figure 1. Identification map of the stars in the field of SAI 63 and SAI 75. North is upwards, east is on the left. Filled circles of different sizes represent the brightness of the stars. The smallest size denotes stars of $V \sim 20$ mag. The open circle represents the cluster size.

Table 3. Calibration coefficients for SAI 63 and SAI 75.

	SAI 63	SAI 75
A_0	8.26 ± 0.01	7.92 ± 0.01
A_1	-0.09 ± 0.02	-0.11 ± 0.02
B_0	5.98 ± 0.01	5.64 ± 0.01
B_1	-0.03 ± 0.01	-0.03 ± 0.01
C_0	5.53 ± 0.01	5.21 ± 0.01
C_1	-0.05 ± 0.01	-0.06 ± 0.01
D_0	5.77 ± 0.01	5.49 ± 0.01
D_1	-0.03 ± 0.01	-0.06 ± 0.01

where U, B, V and I are the standard magnitudes and u, b, v and i are the instrumental magnitudes. X is the airmass ranges from 1.0 to 1.4 in this observation. Mean extinction coefficients for the site have been used. The errors in zero points and colour coefficients are ∼0.01 mag as shown in Table 3.

The internal errors, as derived from DAOPHOT, in U, B, V and I magnitude are plotted against magnitudes in Fig. 2. This figure shows that the mean error is ≤ 0.02 mag at ∼15, 17 and 18 mag in B, V and I passbands respectively. For B magnitude, errors are ∼0.03, ∼0.05 and ∼0.10 mag in the range of 15–17, 17–18 and 18–19 magnitudes respectively. The errors are ∼0.03 and ∼0.05 mag for the V range of 17–18 and 18–19 magnitudes. For 18–19 I magnitude range, the mean error is ∼0.05 mag. The mean error is ≤ 0.05 mag at $U \sim 14$ mag and reaches up to ∼0.13 mag at $U \sim 18$ mag in the U passband. Photometric global (DAOPHOT + calibration) errors have also been determined by following Patat & Carraro (2001) and is listed in Table 4. For the V filter, the errors are 0.05, 0.10 and 0.13 at $V \sim 17.0$, 19.0 and

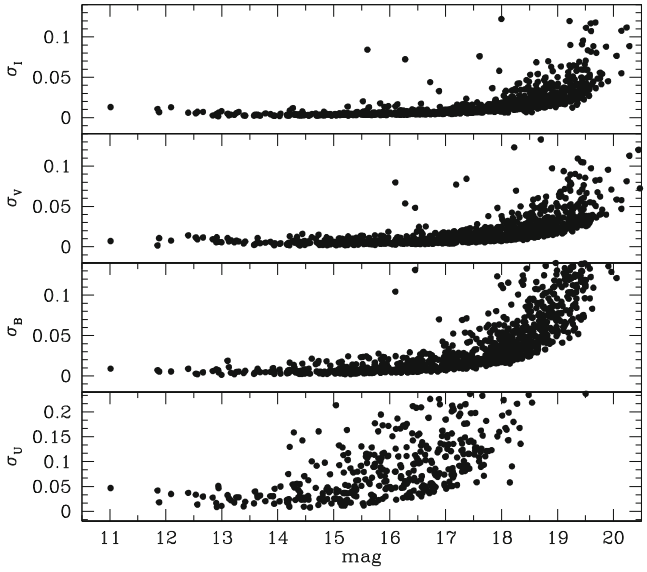

Figure 2. Plot of error in magnitudes as a function of magnitude.

Table 4. The rms global photometric errors as a function of V magnitude.

V mag. range	σ_U	σ_B	σ_V	σ_I
11–13	0.04	0.02	0.02	0.02
13–15	0.06	0.03	0.03	0.03
15–17	0.08	0.05	0.04	0.06
17–19	0.15	0.10	0.10	0.08
19–20		0.15	0.13	0.11

20.0 mag respectively. The final photometric data are available in electronic form at the SAI site[2] and it can also be obtained from the authors.

The X and Y co-ordinates of the stars have been transformed to right ascension and declination of J2000. The Skycat software and Guide Star Catalogue (GSC) at ESO was used to determine an astrometric solution for our data. There were 192 stars common to our data and GSC catalogue. Using the IRAF tasks CCMAP and CCTRAN, we found the corresponding transformation and computed the individual celestial co-ordinates for all the detected stars. The transformations have an rms value of $0''.1$.

3. Analysis of data

3.1 *Size of the clusters*

The Radial Density Profile (RDP) is used to estimate the size of the clusters under study. To determine the radial surface density of stars in a cluster, the imaged area has been divided into a number of concentric circles with respect to the centre given in Table 1 in such a way that each zone contains a statistically significant number of stars. The number of stars in the innermost and outermost zones are 32 and 110 for SAI 63 and 29 and 155 for SAI 75 respectively. The number density of stars, $\rho_i = N_i/A_i$, where N_i is the number of stars and A_i is the area of the i-th zone. The density versus radius plots for SAI 63 and SAI 75 are shown in Fig. 3. A clear radius-density gradient present in Fig. 3 confirms the existence of clustering. Following Bonatto & Bica (2009), we fit the RDP with

$$\sigma(r) = \sigma_{\rm bg} + \frac{\sigma_0}{1 + (r/r_{\rm c})^2}$$

where $\sigma_{\rm bg}$ is the background density, σ_0 is the central density of stars, and $r_{\rm c}$ is the core radius. This function is similar to that introduced by King (1962) to describe the surface brightness profiles in the central parts of globular clusters. The shaded regions in Fig. 3 represent the background density level present in the cluster region. We fit this function to the observed data points for both the clusters and use a χ^2-minimization technique to determine $r_{\rm c}$, σ_0 and $\sigma_{\rm bg}$. As seen in Fig. 3, the fitting of the function shown with dotted line is satisfactory. The best fit solution provides the values and uncertainties in $\sigma_{\rm bg}$, σ_0 and $r_{\rm c}$, and the same are listed in Table 5 for both the clusters. The core radii are 1.3 ± 0.2 and 1.2 ± 0.5 arcmin for the SAI 63 and

[2] http://ocl.sai.msu.ru

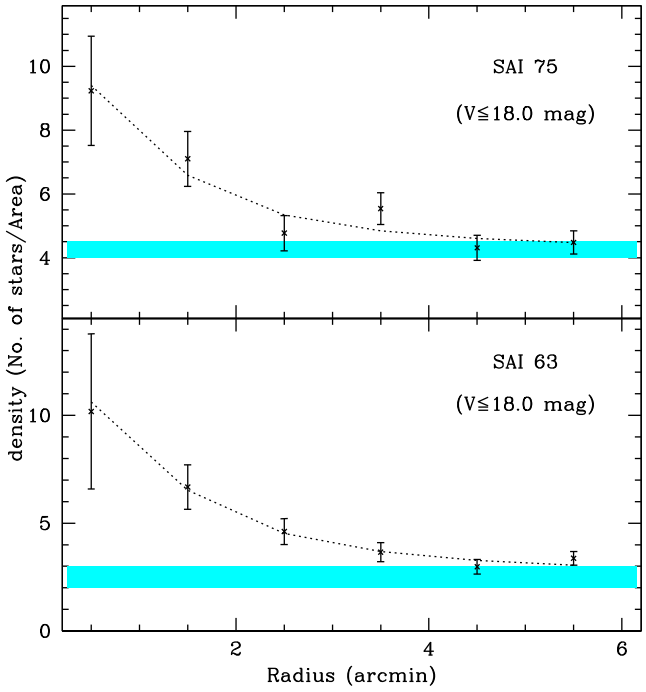

Figure 3. The radial density profile for SAI 63 and SAI 75. The length of the error bar denotes error resulting from sampling statistics ($=1/\sqrt{N}$, where N is the number of stars used in the density estimation at that point). The dotted curves represent the fitted profile whereas shaded region represents the background density level. The width of the background density level shows the error in its determination.

SAI 75 clusters respectively. We also estimated the cluster radius, i.e. the distance from the centre where the cluster RDP and field fluctuations are statistically indistinguishable. The stars outside 1.5 times the radius listed in Table 1 are considered to determine the field star density. The RDP indicates that the radius of the cluster is ∼3.5 and 2.5 arcmin for the SAI 63 and SAI 75 clusters respectively. Our derived value of radius is more than the value listed in Table 1. Present estimate of radii are better because it is determined by using more number of stars.

The density contrast parameter $\delta_c = 1 + \sigma_0/\sigma_{bg}$ is estimated for both the clusters and are listed in Table 5. Present estimate of δ_c for SAI 63 and SAI 75 is lower than the values $7 \leq \delta_c \leq 23$ as expected from compact star clusters (Bonatto & Bica 2009).

Table 5. The derived values of core radius r_c, central density σ_0 and background density σ_{bg} for SAI 63 and SAI 75. Densities are in no. of star/arcmin^2 unit.

Objects	Radius (arcmin)	r_c (arcmin)	σ_0	σ_{bg}	δ_c
SAI 63	3.5	1.3 ± 0.2	9.3 ± 0.8	2.6 ± 0.3	∼4.5
SAI 75	2.5	1.2 ± 0.5	6.1 ± 1.4	4.2 ± 0.5	∼2.5

3.2 *Apparent colour–magnitude diagrams*

In Fig. 4 we present V, $(B - V)$ photometric colour–magnitude diagram of the cluster and field regions for both the clusters under study. Stars falling within the cluster radius are considered as cluster region stars while those outside the radius are field region stars. Field region CMDs for both the clusters are clearly dominated by foreground/background stars.

The CMD constructed by using the stars within the cluster radius for SAI 63 shows a main-sequence (MS) extending from $V \sim 12.5$ to 16.0 mag. After $V = 16.0$ mag it starts merging in the field region stars and is not seen clearly. However, the presence of this cluster seems to be secured by the visibility of MS compared to the field MS. It is difficult to say where the turn-off (TO) is located, but we tentatively identify it at $V \sim 12.5$, $(B - V) \sim 0.5$ mag. We shall estimate the basic parameters of the cluster in the next section.

The CMD of SAI 75 is shown in the right panel of Fig. 4. Stars within the cluster radius are considered to be the cluster region stars. CMD indicates that SAI 75 is a young cluster. A clear MS from $V \sim 12.0$ mag to ~16.0 mag is visible in the cluster area CMD. The MS of the cluster is prominent in comparison to the MS of field stars. MS fainter than 16.0 mag has more scatter and contamination due to field stars is also more evident. Because of this it is hard to delineate cluster members from the field stars only on the basis of their closeness to the main populated area of the CMD. The field star contamination is higher in comparison to the SAI 63 but it does not prevent us from recognizing an open cluster.

To know the frequency distribution of stars in the cluster and field regions we used V, $(B-V)$ CMDs. Members were selected by defining blue and red envelope around the main-sequence which is shown in Fig. 4 for both the clusters. A star is considered as a non-member if it lies outside the marked region in the CMDs. In Table 6, we have listed the expected number of cluster stars and field stars in different magnitude bins. The statistically expected number of cluster members (N_c) show that both the clusters are having poor main-sequence.

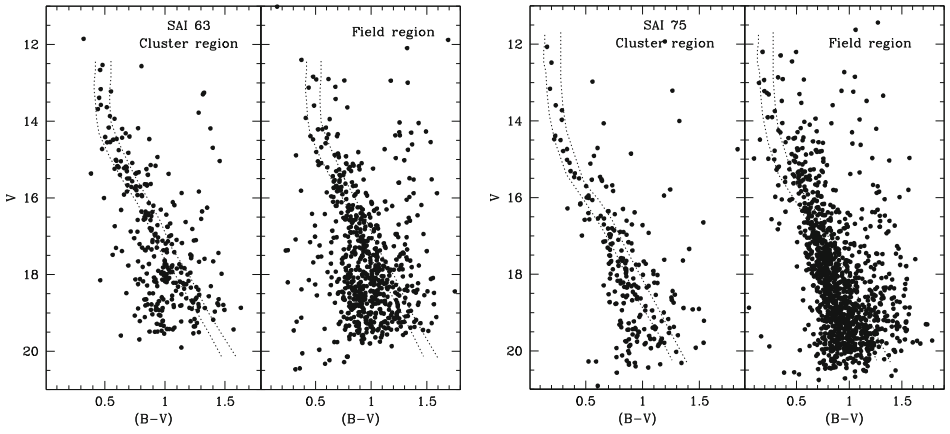

Figure 4. The V, $(B-V)$ CMDs for the clusters SAI 63 and SAI 75 using the stars within the cluster radius (cluster region). Stars outside the cluster radius are also plotted as field region. Dotted lines show the blue and red envelope of the main-sequence.

Table 6. Frequency distribution of the stars in the V, $(B-V)$ diagram of the cluster and field regions. N_B, N_S and N_R denote the number of stars in a magnitude bin blueward, along and redward of the cluster sequence respectively. The number of stars in the field and cluster regions are taken in the same area. N_C (difference between the N_S value of cluster and field regions) denotes the statistically expected number of cluster members in the corresponding magnitude bin.

V range	SAI 63							SAI 75						
	Cluster region			Field region				Cluster region			Field region			
	N_B	N_S	N_R	N_B	N_S	N_R	N_C	N_B	N_S	N_R	N_B	N_S	N_R	N_C
12–13	0	2	1	0	0	2	2	0	2	1	0	1	1	1
13–14	0	6	5	1	2	3	4	0	4	1	1	2	2	2
14–15	1	7	10	1	1	7	6	1	4	5	0	0	5	4
15–16	4	22	16	5	3	7	19	0	8	10	0	2	8	6
16–17	8	15	14	13	7	14	8	7	12	13	3	8	13	4
17–18	33	16	14	36	14	9	2	13	16	12	16	11	10	4
18–19	55	15	12	57	3	13	12	26	10	15	25	10	11	0

3.3 *Reddening of the clusters*

Figure 5 shows the $(U-B)$ versus $(B-V)$ diagrams for estimating the interstellar extinction towards the cluster direction. Stars within the cluster radius and selected in section 3.2 have been used to derive the reddening in the direction of the clusters. We fit the intrinsic Zero-Age Main Sequence (ZAMS) given by Schmidt-Kaler (1982) assuming the slope of reddening $E(U-B)/E(B-V)$ as 0.72. Visual fitting provides the value of $E(B-V) = 0.44 \pm 0.05$ mag for the cluster SAI 63 and $E(B-V) = 0.34 \pm 0.05$ mag for the cluster SAI 75. Our reddening estimates for the imaged region of the cluster SAI 63 agrees well within the error while it is more for the cluster SAI 75 (see Table 1).

3.4 *Interstellar extinction in near-IR*

To study the interstellar extinction in near-IR region, we combine our optical data with 2MASS near-IR JHK_s data. Only good accuracy photometric data ($K_{\rm error}$

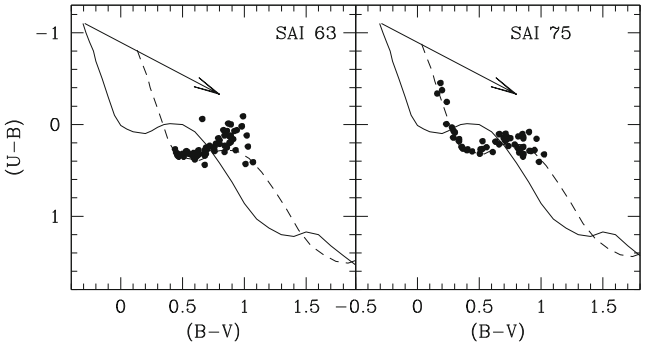

Figure 5. The $(U-B)$ versus $(B-V)$ diagrams of the stars in the cluster region for SAI 63 and SAI 75. The continuous curve represents the locus of Schimidt-Kaler's (1982) ZAMS while the dashed lines are the same ZAMS shifted by the values given in the text. The solid arrow indicates the reddening vector.

≤ 0.08) were used in the present analysis. The K_s magnitudes were converted to K magnitudes following Persson *et al.* (1998). The $(J-K)$ versus $(V-K)$ diagram for both the clusters is shown in Fig. 6. The stars plotted in this diagram are within the cluster's radius and selected in section 3.2. The ZAMS taken from Caldwell *et al.* (1993) is shown with the dotted line. The visually fitted ZAMS gives $E(J-K) = 0.23 \pm 0.05$ and $E(V-K) = 1.30 \pm 0.07$ for SAI 63 and $E(J-K) = 0.17 \pm 0.05$ and $E(V-K) = 1.00 \pm 0.08$ for SAI 75. The ratio $E(J-K)/E(V-K) = 0.18 \pm 0.05$ and 0.17 ± 0.05 for SAI 63 and SAI 75 respectively, are in good agreement with the normal interstellar extinction value of 0.19 given by Cardelli *et al.* (1989).

3.5 *Evaluation of age and distance*

Age and distance of the clusters are estimated by visually fitting the theoretical stellar evolutionary isochrones provided by Girardi *et al.* (2000) for $Z = 0.019$. The detailed shape and position of the different features in the CMD depend mostly on the age and metallicity of the clusters.

SAI 63: We show the fitting of isochrones to V_0, $(U-B)_0$; V_0, $(B-V)_0$ and V_0, $(V-I)_0$ intrinsic CMDs in Fig. 7 using the reddening derived in section 3.3 and normal interstellar extinction law. To reduce the field star contamination we plotted only those stars located within the cluster radius and selected in section 3.2. Three isochrones of log(age) = 8.60, 8.65 and 8.70 and $Z = 0.019$ have been superimposed on the CMDs. The overall fit of isochrones with CMDs is good. The detailed shape of MS and TO are reproduced. The best fitting isochrone provides log(age) = 8.65 ± 0.05. The inferred distance modulus $(m-M)_0 = 11.7 \pm 0.2$ mag provides a heliocentric distance of 2.2 ± 0.2 kpc. The galactocentric distance is 10.5 kpc which is determined by assuming 8.5 kpc as the distance of the Sun to galactic centre. This cluster is nearer to SAI 75. Our distance estimate agrees well within the error with the value listed in Table 1. The galactocentric co-ordinates are $X = -830$ pc,

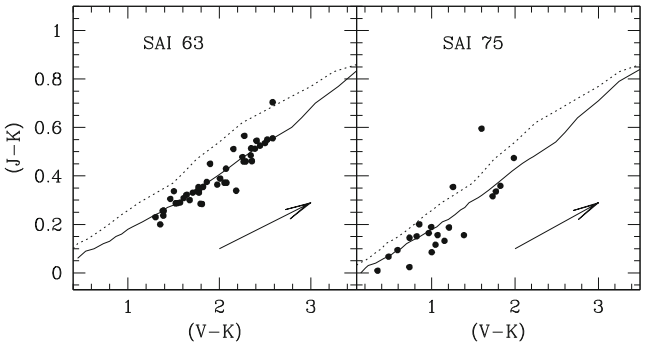

Figure 6. The $(J-K)$ versus $(V-K)$ colour–colour diagram of the clusters under study. Stars shown in the diagram are as selected in section 3.2 and within the cluster's radius. The dotted line is the ZAMS taken from Caldwell *et al.* (1993) while solid line is the same ZAMS shifted by the values provided in the text. The arrow lines represent the reddening vectors.

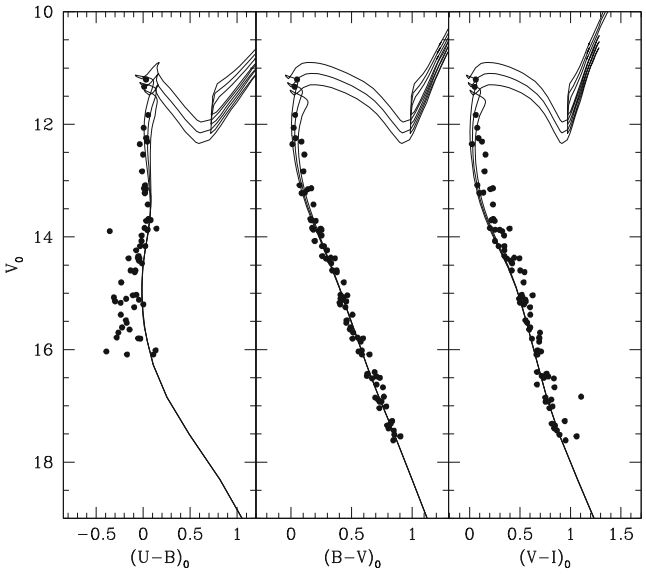

Figure 7. The V_0, $(U-B)_0$; V_0, $(B-V)_0$ and V_0, $(V-I)_0$ reddening corrected CMDs for the cluster SAI 63 using stars within the cluster radius and selected in section 3.2. The solid lines are isochrones taken from Girardi *et al.* (2000). Three isochrones of different age and $Z = 0.019$ are shown in the CMDs.

$Y = 2020$ pc and $Z = -200$ pc. The value of Z indicates that this cluster is in the lower part of the galactic disk.

SAI 75: The CMD shown in Fig. 4 for this cluster resembles a young cluster. To estimate the age and distance of this cluster we selected the photometric members using $(U-B)$, $(B-V)$ and V, $(B-V)$ diagrams. Individual reddening values have been estimated by means of the usual reddening free parameter $Q = (U-B) - 0.72 \times (B-V)$ method. This method is very useful to isolate early spectral type (from O to A0) having common reddening, which are most probable cluster members.

In Fig. 8, we construct the reddening corrected CMDs in $(U-B)_0$ versus V_0 and $(B-V)_0$ versus V_0 planes for all the stars for which we could obtain a reddening estimate. Stars seem to form a tight sequence, confirming that they are good candidate members. Overimposed is the empirical ZAMS (dotted lines) given by Schmidt-Kaler (1982), and shifted by $(m-M)_0 = 12.7$ mag. The same ZAMS has been shifted by 0.70 mag (long dash line) to have an idea of the MS broadening due to unresolved binaries. We can readily see that most of the member stars fall close to the ZAMS location. The ZAMS shifted by $(m-M)_0 = 12.7 \pm 0.2$ provides a good fit to the bulk of the stars and implies that SAI 75 is located 3.5 $\pm$0.3 kpc away from the Sun. This cluster is located at 11.3 kpc from the galactic centre. The galactocentric co-ordinates are $X = -2350$ pc, $Y = 2600$ pc and $Z = 115$ pc. The Z indicates that this object is in the upper part of the galactic disk.

We represent the $(B-V)$ vs. $(U-B)$ two colour diagram for SAI 75 in Fig. 5. Based on the position of the photometric members in the diagram, the photometric

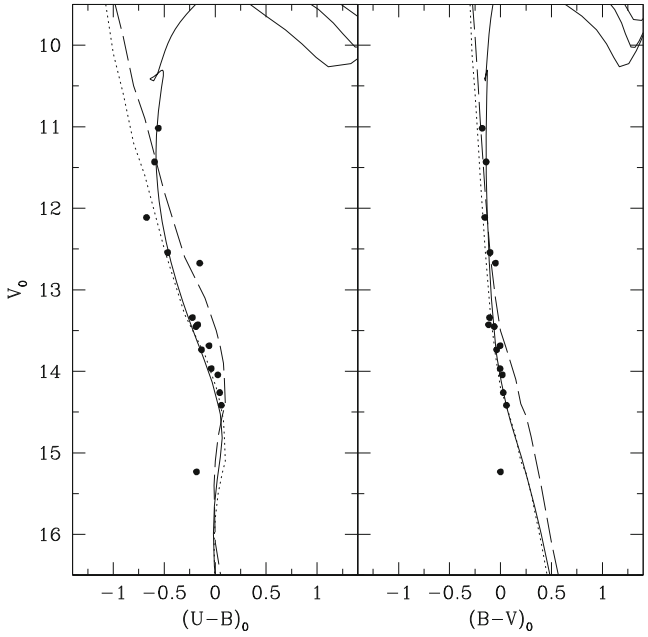

Figure 8. The reddening corrected CMDs in $(U-B)_0$ versus V_0 and $(B-V)_0$ versus V_0 planes for the cluster SAI 75. The solid lines are isochrones taken from Girardi *et al.* (2000) while dotted lines are the ZAMS taken from Schmidt-Kaler (1982).

spectral type of the brightest member can be determined as $B5$. If the $B5$ spectral type star is still present on the MS, we can derive an age around 1×10^8 years for SAI 75. We checked this age estimate by fitting the theoretical isochrone of $Z = 0.019$ given by Girardi *et al.* (2000) in $(B-V)_0$, V_0 and $(U-B)_0$, V_0 CMD. The isochrone superimposed in the intrinsic CMD is presented in Fig. 8 by dashed line. This isochrone is for the log(age) = 7.95. The overall fit is good in both the diagrams. This estimated age is in good agreement with the value derived using spectral type. Therefore, we conclude that SAI 75 is a young open cluster of log(age) = 7.95 ± 0.05.

3.6 *Colour excess diagram*

In Fig. 9, we plot a colour-excess diagram to study the interstellar extinction law towards the cluster SAI 75 using optical and near-IR data. For this analysis, we selected the stars earlier than A0 spectral type by using colour–colour and colour–magnitude diagrams. We could not perform this analysis for SAI 63 due to the unavailability of early type stars in this cluster. The colour-excesses have been determined by comparing the colour of stars with intrinsic colours derived from the colour relations given by FitzGerald (1970) for $(U-B)$ and $(B-V)$; Johnson & Morgan (1966) for $(V-I)$ and Koornneef (1983) for $(V-J)$, $(V-H)$ and $(V-K)$. The colour excess $E(U-B)$, $E(B-V)$, $E(V-I)$, $E(V-J)$, $E(V-H)$ and $E(V-K)$ are plotted against $E(B-V)$ in Fig. 9. The solid straight line shown in

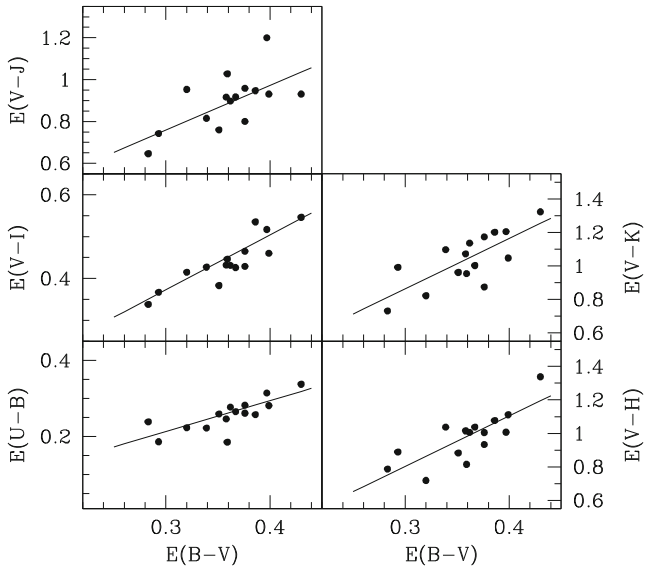

Figure 9. The plot of $E(U-B)$, $E(V-I)$, $E(V-J)$, $E(V-H)$ and $E(V-K)$ versus $E(B-V)$ colour-excess diagram of the cluster SAI 75. The solid straight lines represent the least-squares linear fit to the data points.

the figure is the least-squares linear fit to the data points. The fit in all colour excess diagram indicates that data points are well represented by a linear relation. Scattering is more pronounced in the colour excess $E(V-J)$, $E(V-H)$ and $E(V-K)$ because of large errors in *JHK* magnitudes. In Table 7, we have listed the slope of the straight lines that represent the reddening directions in the form of colour excess ratios. The normal colour excess ratios given by Cardelli *et al.* (1989) are also listed in Table 7. The present colour excess ratios in the direction of SAI 75 generally agree within 2σ error with those given for normal interstellar extinction law. This indicates that the interstellar extinction law is normal in the direction of SAI 75.

Furthermore, to understand the nature of extinction law, we have determined the value of R. We use the relation $R = 1.1\frac{E(V-K)}{E(B-V)}$ given by Whittet & van Breda (1980), which is used for longer wavelengths. In this way we determined the value of $R \sim 3.3$, which in agreement with the value of 3.1 for the normal extinction law.

Table 7. A comparison of the extinction law in the direction of the cluster SAI 75 with a normal extinction law given by Cardelli *et al.* (1989).

Objects	$\frac{E(U-B)}{E(B-V)}$	$\frac{E(V-I)}{E(B-V)}$	$\frac{E(V-J)}{E(B-V)}$	$\frac{E(V-H)}{E(B-V)}$	$\frac{E(V-K)}{E(B-V)}$
Normal	0.72	1.60	2.22	2.55	2.74
SAI 75	0.81 ± 0.18	1.31 ± 0.19	2.13 ± 0.70	3.01 ± 0.65	3.01 ± 0.75

Table 8. The derived fundamental parameters of the clusters considered in the present study. X, Y and Z are the galactocentric co-ordinates and R_{GC} is the galactocentric distance of the clusters. The co-ordinate system is such that the Y-axis connects the Sun to the galactic centre, while the X-axis is perpendicular to that. Y is positive in the anticentre direction, and X is positive in the first and second galactic quadrants (Lynga 1982).

Objects	$E(B-V)$ (mag)	Distance (kpc)	X (pc)	Y (pc)	Z (pc)	R_{GC} (kpc)	log(age)
SAI 63	0.44 ± 0.05	2.2 ± 0.2	-830	2020	-200	10.5	8.65 ± 0.05
SAI 75	0.34 ± 0.05	3.5 ± 0.3	-2350	2600	115	11.3	7.95 ± 0.05

4. Conclusions

In this paper we presented *UBVI* CCD photometry for the two open clusters SAI 63 and SAI 75. The result is summarized in Table 8. Our results can be summarized as follows:

(1) The radial density profiles of the clusters indicate the existence of grouping. The radius of the clusters SAI 63 and SAI 75 are 3.5 and 2.5 arcmin respectively. The corresponding linear sizes are 2.2 and 2.5 pc respectively.
(2) Using two color diagram $(U-B)$ versus $(B-V)$, we estimated $E(B-V) = 0.44 \pm 0.05$ for SAI 63 and 0.34 ± 0.05 for SAI 75. The *JHK* data in combination with the optical data provide $E(J-K) = 0.23 \pm 0.05$ and $E(V-K) = 1.30 \pm 0.07$ for SAI 63 and $E(J-K) = 0.17 \pm 0.05$ and $E(V-K) = 1.00 \pm 0.08$ for SAI 75 respectively.
(3) Distances to the clusters are determined as 2.2 ± 0.2 and 3.5 ± 0.3 kpc for SAI 63 and SAI 75 respectively. An age of 450 ± 50 Myr for SAI 63 and 90 ± 10 Myr for SAI 75 is determined by comparing the isochrones of $Z = 0.019$ given by Girardi *et al.* (2000) using reddening corrected colour–magnitude diagrams.
(4) Colour excess diagram for SAI 75 shows that cluster members generally follow the normal interstellar extinction law.

Acknowledgements

This work has been financially supported by the Department of Science and Technology India (Project No. INT/RFBR/P-40) and by the Russian Foundation for Basic Research (Project No. 09-02-92669-IND-a). The authors are grateful to Mr. Devesh P. Sariya for his help during observations. This publication makes use of data products from the Two-Micron All Sky Survey, which is a joint project of the University of Massachusetts and the Infrared Processing and Analysis Center/ California Institute of Technology, funded by the National Aeronautics and Space Administration and the National Science Foundation.This research has made use of the SIMBAD database, operated at CDS, Strasbourg, France.

References

Bonatto, C., Bica, E. 2009, *MNRAS*, **397**, 1915.
Caldwell, J. A. R., Cousins, A. W. J., Ahlers, C. C., van Wamelen, P., Maritz, E. J. 1993, South African Astron. Observatory, Circ. No. 15.

Cardelli, J. A., Clayton, G. C., Mathis, J. S. 1989, *ApJ*, **345**, 245.
Carraro, G., Beletsky, Y., Marconi, G. 2013, *MNRAS*, **428**, 502.
FitzGerald, M. P. 1970, *A&A*, **4**, 234.
Froebrich, D., Scholz, A., Raftery, C. L. 2007, *MNRAS*, **374**, 399.
Girardi, L., Bressan, A., Bertelli, G., Chiosi, C. 2000, *A&AS*, **141**, 371.
Glushkova, E. V., Koposov, S. E., Zolotukhin, I. Yu., Beletsky, Yu. V., Vlasov, A. D., Leonova, S. I. 2010, *Astron Lett.*, **36**, 75.
Johnson, H. L., Morgan, W. W. 1966, *ARA&A*, **4**, 193.
King, I. 1962, *AJ*, **67**, 471.
Koposov, S. E., Glushkova, E. V., Zolotukhin, I. Yu 2008, *A&A*, **486**, 771.
Koornneef, J. 1983, *A&A*, **128**, 84.
Kronberger *et al.* 2006, *A&A*, **447**, 921.
Lynga, G. 1982, *A&A*, **109**, 213.
Landolt, A. U. 1992, *AJ*, **104**, 340.
Patat, F., Carraro, G. 2001, *MNRAS*, **325**, 1591.
Persson, S. E., Murphy, D. C., Krzeminski, W., Roth, M., Rieke, M. J. 1998, *AJ*, **116**, 2475.
Stetson, P. B. 1987, *PASP*, **99**, 191.
Stetson, P. B. 1992, in: Warrall D. M., Biemesderfer C., Barnes J., (eds), ASP Conf. Ser. Vol. 25, Astronomical Data Analysis Software and System I. Astron. Soc. Pac. San Francisco, p. 297.
Schmidt-Kaler, Th. 1982, in: Landolt-Börnstein New Series, Group 6, Vol. 2b, Stars and Star Clusters, Schaifers K., Voigt H.-H. (eds), Springer, Berlin, p. 1.
Whittet, D. C. B., van Breda, I. G. 1980, *MNRAS*, **192**, 467.